Operation of paddy field tillage wheel based on SPH

Xian Zheng, Hongyan Yang, Wang Yang*

(*College of Mechanical Engineering, Guangxi university, Nanning 530004, Guangxi, China*)

Abstract: A new type of paddy field micro-tiller that places the rotary cutter roller in front of the driving wheel has been developed in China. Its driving wheel not only has a driving function, but also has the function of crushing and stirring the soil, so it is called a tillage wheel. However, at present, there are few studies on the wheel's operating mechanism and force and the influences of factors on the wheel's operational performance, which is not conducive to its optimal design. This study verifies the rationality of the soil-tillage wheel system modeling method based on the smoothed particle hydrodynamics method (SPH) through field test. The movement track and force variation of the single-wheel blade in soil as well as the interaction between the single-wheel blade and soil were studied using the established simulation model. Moreover, mathematical models were developed to examine how various factors affect the wheel's operational performance. The results show that the modeling method is reasonable. As the rotation angle of the wheel blade increases, both the horizontal thrust and support force initially rise and then fall. The maximum horizontal thrust at the slip rate of 3.1% is 42.28% smaller than that of 26%. But the maximum support force at the slip rate of 3.1% is 10% greater than that of 26%. When the outer diameter of the wheel, the number of wheel blades, and the inclination angle of the wheel blade are small, as the wheel blade angle increases, the average advance speed increases, and the stirring degree decreases, and vice versa. Using the simulation method to study the wheel's operating mechanism and force and the influences of various factors on the wheel's operational performance is of great significance to the optimization of its design.

Keywords: tillage wheel, single-wheel blade, numerical simulation, operating mechanism, mathematical model, factor influence

DOI: 10.25165/j.ijabe.20241706.8908

Citation: Zheng X, Yang H Y, Yang W. Operation of paddy field tillage wheel based on SPH. Int J Agric & Biol Eng, 2024; 17(6): 176–184.

1 Introduction

A paddy field micro-tiller (hereinafter, micro-tiller) is widely used for tillage in small paddy field areas, and the structure and motion parameters of its driving wheel have a great influence on the driving performance. Therefore, many studies have been conducted on the effects of these parameters using physical tests and theoretical analysis methods[1-5], and the related design theories of the paddy field wheel have been established[6-9].

The micro-tiller that places the rotary cutter roller in front of the driving wheel is a new type of micro-tiller (hereinafter, new micro-tiller). It was invented in China[10] in recent years. Because its driving wheel not only has the driving function of the driving wheel of the general micro-tiller, but also has the function of crushing and stirring soil, its driving wheel is called a "tillage wheel". Compared to conventional micro-tillers with a front driving wheel and rear rotary cutter roller, or those with only a rotary cutter roller, the new micro-tiller completes tillage and land preparation in a single pass, doubling efficiency and maintaining stable tillage depth. The new micro-tiller is mainly composed of support, handrail, engine, gearbox, tillage wheel, rotary cutter roller, and so on. The tillage wheel is composed of a connecting circular plate, spoke, rim, and wheel blade, and its width is the same as the width of the rotary cutter roller. The new micro-tiller and the tillage wheel are shown in Figure 1.

When the new micro-tiller is operated, the handrail is held by the hand, and the engine transmits the power to the tillage wheel and the rotary cutter roller through the reduction box and the transmission mechanism respectively, and the new micro-tiller moves forward under the driving action of the tillage wheel. The rotary cutter roller in front cuts the soil to form clods, and these clods are thrown to the fender and smashed by impact, and then the tillage wheel crushes and stirs the small clods to further break and mix the soil. Therefore, the design method of the tillage wheel and the design method of the driving wheel of the general micro-tiller are different. Simultaneously, the research on the operating mechanism and the influence law of operational performance of the tillage wheel is lacking at present, which is not conducive to its optimal design. Therefore, studying the operating mechanism and performance impact law of the tillage wheel provides a basis for the optimal design of the tillage wheel, which is of great significance for improving the performance of the new micro-tiller.

The operating mechanism of the tillage wheel is complicated, and it is time-consuming and difficult to find out the action process of the tillage wheel and the soil through physical testing. The simulation method is a method for effectively studying scientific problems. At present, the most commonly used numerical methods for soil tillage simulation are the finite element method (FEM)[11,12] or discrete element method (DEM)[13-17]. However, since FEM is a grid-based numerical method, it is easy to generate grid distortion when dealing with large deformation problems of soil, resulting in calculations that do not converge. Therefore, it is more difficult to simulate the real situation of soil fragmentation. DEM has no grid limitation and can effectively simulate the soil tillage process, but

Received date: 2024-03-08 **Accepted date:** 2024-11-13

Biographies: Xian Zheng, PhD candidate, research interest: Research and development of agricultural machinery and equipment, Email: 1140080116@qq.com; **Hongyan Yang**, MS, research interest: agricultural machinery and equipment, Email: 787405443@qq.com.

***Corresponding author: Wang Yang**, PhD, Associate Professor, research interest:Intelligent agricultural machinery equipment. College of Mechanical Engineering, Guangxi university, Nanning 530004, Guangxi, China. Tel: +86-13557210593, E-mail: yanghope@163.com.

the contact parameters are difficult to determine. In recent years, the meshless method has been actively developed and has been applied in simulating large deformations of continuum or dispersion. Among these methods, SPH has the longest research time and is mature compared to other meshless methods. SPH is a pure Lagrangian meshless method in which particles carry field variables such as mass, density, stress tensor, etc., and move with the velocity of the material. Through the SPH, the partial differential equations of the continuum are transformed into the equations of motion of these particles, and then solved by the modified Lagrangian numerical format. Compared with other grid-based numerical methods, SPH has Lagrangian and adaptive characteristics, which can simulate the process of large deformation and fragmentation of soil. At present, this method has also been used in the study of interaction between various tillage tools and soil[18-23]. Therefore, this study used the SPH method to build the simulation model of the operation system on the tillage wheel and conducted research on the operation of the tillage wheel.

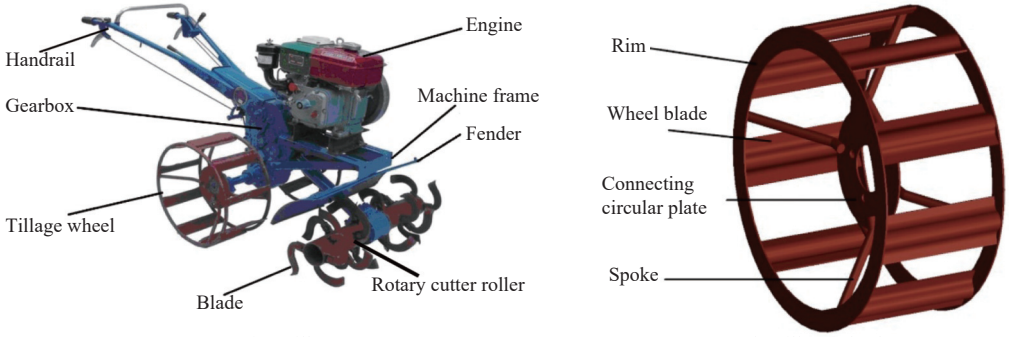

a. New micro-tiller b. Tillage wheel

Figure 1 New micro-tiller and tillage wheel

In this study, field tests were conducted first to measure the sinking depth and slip rate of the tillage wheel at low rotation speeds. By comparing these results with simulation outcomes, the rationality of the modeling method of soil-tillage wheel system based on SPH method was verified. Then, using the established simulation model, the movement of wheel blade in soil, the interaction between wheel blade and soil, and the force of wheel blade were studied. Simultaneously, using the quadratic regression orthogonal rotation test design, simulation test, and regression analysis method, the mathematical model of the operational performance of the tillage wheel affected by multiple factors was established, and it revealed the influence law of its operational performance. The aim is to improve the theory of tillage wheel design and provide a theoretical basis for the optimization of its design.

2 Materials and methods

2.1 Test site

The test site was the paddy field of Guangxi University Farm (22.8°N, 108.3°E). The soil was silty loam. The field investigation before the test showed that the soil properties of the soft soil layer (upper layer) and the hard soil layer (lower layer) of the test site were greatly different. Therefore, the soil physical property parameters of the upper and lower layers were measured separately. The soil thickness of the soft soil layer was about 10 cm. The soil parameters were measured by the test methods found in the relevant literature[24-26]. The measured soil parameters are listed in Table 1.

Table 1 Soil parameters

Soil properties	Soil layer	
	Upper soil	Lower soil
Density/kg·m^{-3}	1624.96	1894.50
Elastic modulus/Pa	0.2×10^{6}	1.0×10^{6}
Bulk modulus/Pa	1.667×10^{5}	8.333×10^{5}
Shear modulus/Pa	7.690×10^{4}	3.846×10^{5}
Internal friction angle/°	2.5844	4.0954
Cohesion/kPa	7.0012	14.8640
Moisture content/%	42.95	28.1
Soil-metal friction coefficient	0.3	0.5

2.2 Field test method

In the field test, when measuring the sinking depth and slip rate of the tillage wheel, in order to facilitate the measurement of the rotation speed of the tillage wheel, its rotation speed was controlled to be in a low rotation state. This was achieved by selecting the speed gear position and adjusting the accelerator. Simultaneously, in order to facilitate the analysis, when the new micro-tiller advanced, the handrail was operated to lift the rotary cutter roller off the ground without working (no load).

When the new micro-tiller is operating in the paddy field, it is difficult to directly measure the rotation speed of the tillage wheel shaft. Therefore, this study first used the infrared tachometer (Guangzhou Qing Mai Electronics Co., Ltd., China) to measure the rotation speed of the pulley, and then calculated the rotation speed of the tillage wheel according to the transmission ratio of the reduction gearbox. The sinking depth of the tillage wheel was measured directly with a ruler. The slip rate of the tillage wheel was measured by conventional methods. That is to say, the number of rotations of the tillage wheel when the new micro-tiller advances the L_1 distance was measured, and then the theoretical advance distance L of the new micro-tiller was calculated according to the number of rotations and the radius of the tillage wheel. Finally, the slip rate (%) was calculated from Equation (1).

$$\delta = \frac{L - L_1}{L} \times 100 \tag{1}$$

The field measurement was repeated six times. Main equipment included 1WGQ4-type new micro-tiller (transmission ratio: first gear 38.5, second gear 23, reverse gear 50) (Guangxi Luzhou Machinery Manufacturing Co., Ltd., China), infrared tachometer, tape measure, and ruler. The test site is shown in Figure 2.

Figure 2 Test site

2.3 Numerical simulation model

2.3.1 Geometric model

The stiffness of the tillage wheel is significantly greater than that of the soil, and the wheel blade is approximately cuboidal in shape. Therefore, in order to save simulation calculation time and facilitate modeling, the tillage wheel was modeled as a rigid body, and the following simplification was made to the tillage wheel shown in Figure 1b:

1) The connecting circular plate and spokes were eliminated. Only the rim and wheel blades were retained.

2) The wheel blade was simplified into a cuboid.

The simplified model of the tillage wheel is shown in Figure3. Figure 4 is a schematic diagram of the structural parameters of the tillage wheel. According to the actual dimensions of the tillage wheel prototype, the dimensions of the model were determined. The outer diameter d_1 of the rim is 450 mm, the inner diameter d_2 is 420 mm, and the thickness is 5 mm. The length b of the wheel blade is 240 mm, the width a is 72 mm, and the thickness is 6 mm. The inclination angle γ of the wheel blade is 45°.

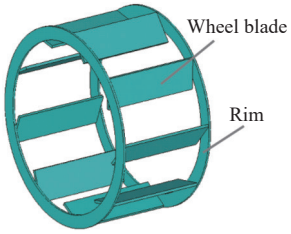

Figure 3 Simplified model of tillage wheel

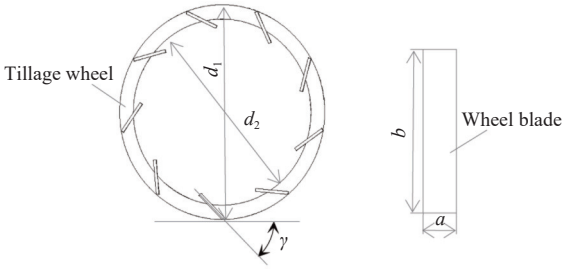

Note: d_1: outer diameter of rim; d_2: inner diameter of rim; γ: inclination angle of wheel blade; b: length of wheel blade; a: width of wheel blade

Figure 4 Schematic diagram of structural parameters of tillage wheel

Because the left and right tillage wheels are symmetrical, the effect of the left and right sides of each tillage wheel on the soil is also the same. Therefore, in order to reduce the simulation time, only the 1/2 tillage wheel model was built for simulation studies. The soil model was built into a cuboid. The width of the soil model should be larger than the width of the 1/2 tillage wheel. The length of the soil model should meet the requirements of the simulation test analysis. Therefore, the size (length×width×height) of the soil model selected in this paper was 155 cm×19.5 cm×14 cm. Simultaneously, according to the measured soil conditions in the field, the soil was divided into two layers for modeling, and the thickness of the upper soft soil was taken as 10 cm. According to Yang et al.[26], without changing the interaction between the wheel and soil, the thickness of the lower soil was taken as 4 cm. The geometric model of the established soil-tillage wheel system is shown in Figure 5.

2.3.2 Material model

In this study, the commercial software LS-DYNA was used to simulate the operation process of the tillage wheel. The tillage wheel was modeled using a hexahedral element of LS-DYNA (Livermore Software Technology Corporation, China) and was defined as a rigid material. Since the spokes and the connecting circular plate were omitted when modeling, the material density increased moderately to maintain the original mass. The material parameters are as follows: the density is 1.112×10^4 kg/m^3, Poisson's ratio is 0.27, and the elastic modulus is 0.2×10^{12} Pa[23].

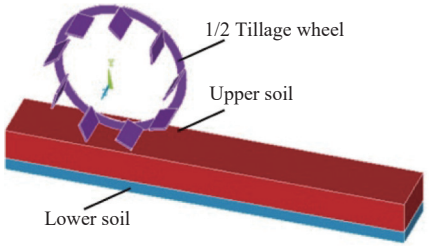

Figure 5 Geometric model of soil-tillage wheel system

The soil was modeled using SPH element. The constitutive relation of soil has a great influence on the accuracy of the simulation results of the tillage process[27,28]. To enhance simulation accuracy, this study referred to the relevant literature[25] and selected MAT_FHWA_SOIL in LS-DYNA as the material model of soil. The model considers the effects of moisture content, strain softening, strain rate effect, void ratio, and pore water pressure, and obeys the modified Mohr-Coulomb yield criterion.

$$F=-P\sin\varphi+\sqrt{J_2K^2(\theta)+A^2\sin^2\varphi}-c\cos\varphi=0 \quad (2)$$

where, P is the hydrostatic pressure value; φ is the internal friction angle; J_2 is the second invariant of stress partial tensor; $K(\theta)$ is a function of the tensor plane angle; A is the D-P coefficient; c is cohesion.

The relevant material parameters for establishing the soil model were the same as those of the experimental site.

2.3.3 Meshing, loading, and boundary

The tillage wheel was meshed using the smart size algorithm in ANSYS (ANSYS Corporation, China)[29]. The number of elements of the tillage wheel was 12 010. The rectangle soil models were meshed using the mapping method. The number of elements of the upper soil and the lower soil were 33 033 and 15 015, respectively.

The total mass of the 1WGQ4-type new micro-tiller is 157 kg. The mass of two tillage wheels is 14 kg. Meanwhile, when the rotary cutter roller leaves the ground and the 1WGQ4-type new micro-tiller moves forward normally, a vertical downward force and a horizontal backward force were applied on the handrail. These two forces were measured by attaching a spring tension gauge (Leqing Edebao Instrument Co., Ltd., China) to the handle position in the field. The measured vertical and horizontal forces were 210 N and 140 N, respectively. Therefore, the vertical downward force of 402.85 N and the horizontal backward force of 35 N were applied on the mass center of the 1/2 tillage wheel. The calculation of the vertical downward force was obtained according to the following formula:

$$\frac{(m_1-m_2)\times g+F_V}{4}=\frac{(157-14)\times9.8+210}{4}=402.85\,(\mathrm{N}) \quad (3)$$

where, m_1 is the total mass of the 1WGQ4-type new micro-tiller; m_2 is the mass of two tillage wheels; g is the gravitational acceleration; F_V is the measured vertical force.

The calculation of the horizontal backward force was obtained according to the following equation:

$$F_H/4 = 140/4 = 35\,(\mathrm{N}) \quad (4)$$

where, F_H is the measured horizontal force.

And in order to verify the simulation model, the rotational speed imposed on the tillage wheel model was the same as the rotational speed of the field trial. The contact between the soil and the tillage wheel was defined by the node surface contact. At the same time, in order to analyze the forces of the single-wheel blade, the contact of one of the wheel blades with the soil was defined separately. Since only the operating system model of the 1/2 tillage wheel was established, the particles in the vicinity of the symmetry boundary surface were treated using the "virtual particle" method when defining the symmetrical boundary conditions[21]. All soil boundaries, except the upper surface and the plane of symmetry, were fully constrained.

2.3.4 Model verification

First, field experiments were conducted to measure the sinking depth and slip rate of the tillage wheel under no-load conditions. The soil-tillage wheel system modeling method, based on the SPH method, was then validated by comparing these results with simulation experiments. The slip rate in the simulation was also calculated according to Equation (1), but L_1 is the moving distance of the wheel in the simulation.

2.4 Design of simulation test

In the simulation test, in order to obtain the actual influence law, it is necessary to consider the force required for the tillage wheel to push the rotary cutter roller forward. The method for determining the force was as follows: First, use the physical test method in Section 2.2 to measure the slip rate of the wheel under load (when the rotary tiller blade of the micro-tiller is working). Repeat the test six times, then take the average value. Then, using the established soil-tillage wheel simulation model and applying the horizontal resistance (under load) on the wheel, obtain the slip rate in the simulation. Next, referring to the reverse calculation method in the literature[24], by changing the applied horizontal resistance in the simulation model, the slip rate in the simulation approximates the slip rate in the physical test, and thus calculate the horizontal resistance, with a magnitude of 415 N. Finally, apply a horizontal resistance of 415 N to the center of mass of the 1/2 tillage wheel model. The rotation speed of the tillage wheel is the rotational speed ω (3.25 rad/s) at the rated power of the first gear of the physical test prototype.

The simulation test was carried out with quadratic regression rotation design method. According to the situation of the tillage wheel, the outer diameter d_1, width a, wheel blade inclination angle γ, and the number of wheel blades n were chosen as test factors. However, the preliminary simulation test showed that the break angle of the wheel blade (referred as wheel blade angle) had a great influence on the operational performance. Therefore, the wheel blade angle θ was also selected as a test factor. The wheel blade with wheel blade angle and its parameters are shown in Figure 6.

Wherein, the arc line s is the outer circle of the wheel, and the straight line l is the connecting line between the ends of the wheel blade (the wheel blade reference line). The inclination angle γ of the wheel blade and the width a of the wheel blade are defined by the reference line. The angle between the reference line and the tangential line of the outer circle of the wheel is the inclination angle of the wheel blade. The projection length of the wheel blade on the reference line is the width of the wheel blade. e is the short side of the wheel blade. If e is small, the effect of excavating the soil is poor, and if e is too large, the ability to excavate the soil is too strong, and the soil splash is too high. Therefore, this study has taken e as 20 mm and treated it as a fixed value. The included angle between the long side and the short side extension line of the wheel blade is the wheel blade angle θ. According to the actual situation of the tillage wheel and the previous test, the numerical ranges of the test factors were determined. Among them, d_1 was 400-540 mm, a was 50-90 mm, γ was 25°-65°, θ was 0°-30°, and n was 6-14 pieces.

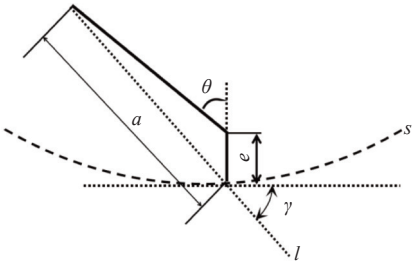

Figure 6 Wheel blade with wheel blade angle and its parameters

When the new micro-tiller is operating, the average forward speed reflects the operational efficiency. Currently, the broken soil performance and the stirring soil performance in paddy fields do not have an accurate metric. However, the stirring degree (ratio of the number of particles leaving the original soil layer to the total number of particles) can relatively reflect the effect of the crushing and stirring of the tillage wheel on the soil. Therefore, the simulation test design in this study selects the average forward speed y_1 and the stirring degree y_2 as test indicators. In the simulation test, in order to facilitate the observation of the effect of the tillage wheel on the soil and the calculation of the stirring degree, the soil of upper layer was divided into two layers, defined as different colors. The simulation diagram of tillage wheel operation is shown in Figure 7.

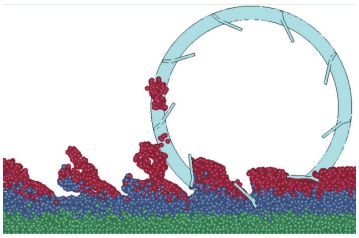

Figure 7 Simulation diagram of tillage wheel operation

See Appendix A for the test plan. According to the factor combination of different test numbers in the test plan of Appendix A and the above modeling methods, different simulation models of the tillage wheel operating system are constructed for simulation test.

3 Results and discussion

3.1 Model verification

In the field test of the condition of no-load and rotation speed of 1.8 rad/s, the average sinking depth of the tillage wheel was about 8 cm. The average slip rate was 3.21%, as seen in Table 2. In the simulation test, when the tillage wheel ran stably, the average sinking depth was also about 8 cm, as seen in Figure 8. The slip rate was 3.1%. That is, the average slip rate relative error of the field test and the simulation test is 3.4%, and the average sinking depth is the same. Moreover, the wheel rut observed in the simulation matched that of the field test (see Figure 9). These results confirm that the modeling method of the soil-tillage wheel system based on SPH method is reasonable, and the established model is suitable for simulating tillage wheel operations.

Table 2 Test results of slip rate

Test number	Laps of wheel turning/r	Measured forward distance/cm	Theoretical forward distance/cm	Slip rate/%	Physical average slip rate/%
1	4	548	565.2	3.0	
2	4	550	565.2	2.69	
3	4	546	565.2	3.40	3.21
4	4	542	565.2	4.10	
5	4	549	565.2	2.87	
6	4	547	565.2	3.22	

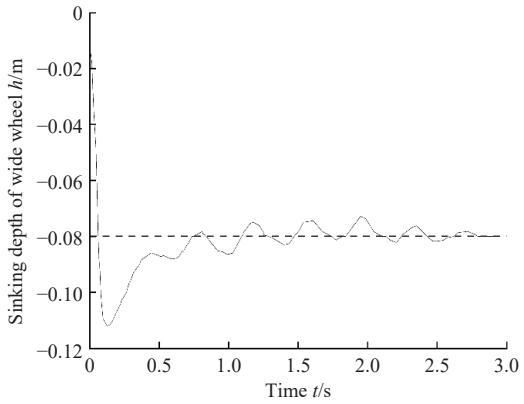

Figure 8 Sinking depth curve of tillage wheel in simulation experiment

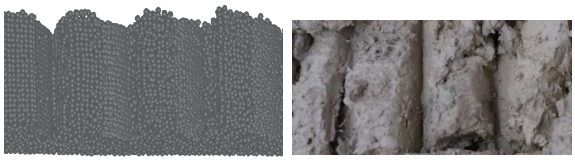

a. Wheel rut of simulation test b. Wheel rut of field test

Figure 9 Wheel rut after interaction between tillage wheel and soil

3.2 Operation process of single-wheel blade

Figures 10 and 11 are simulated screenshots of the movement of the single-wheel blade in the soil. Among them, Figure 10 is a simulated screenshot of the slip rate of 3.1% (no load), and Figure 11 is a simulated screenshot of the slip rate of 26% (backward plus horizontal load 415 N). The curve in the figure is the trajectory of the front and rear ends of the wheel blade. α is the angle of rotation of the wheel blade around the wheel center after the wheel blade contacts the topsoil.

It can be seen from Figure 10 and 11 and the simulation process that when the slip rate of tillage wheel is 3.1%, the front end track of the wheel blade is a small long cycloid, and the backend track is a short cycloid. When the slip rate is 26%, the trajectories of the front end and back end of the wheel blade are long cycloid, but the long cycloid of the front end is large. First, with the increase of α, the wheel blade gradually moves backward and downward. The soil behind and below the wheel blade is squeezed gradually, the soil stress is gradually increased to the maximum value, and the elastoplastic deformation of the soil is gradually increased. The soil

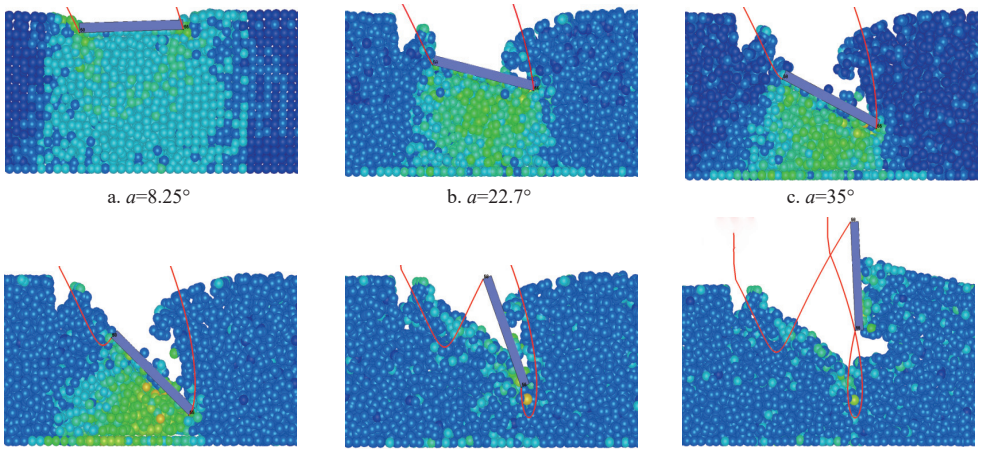

a. a=8.25° b. a=22.7° c. a=35°

d. a=51.57° e. a=78.38° f. a=97°

Figure 10 Screenshot of motion simulation of wheel blade in soil when slip ratio is 3.1%

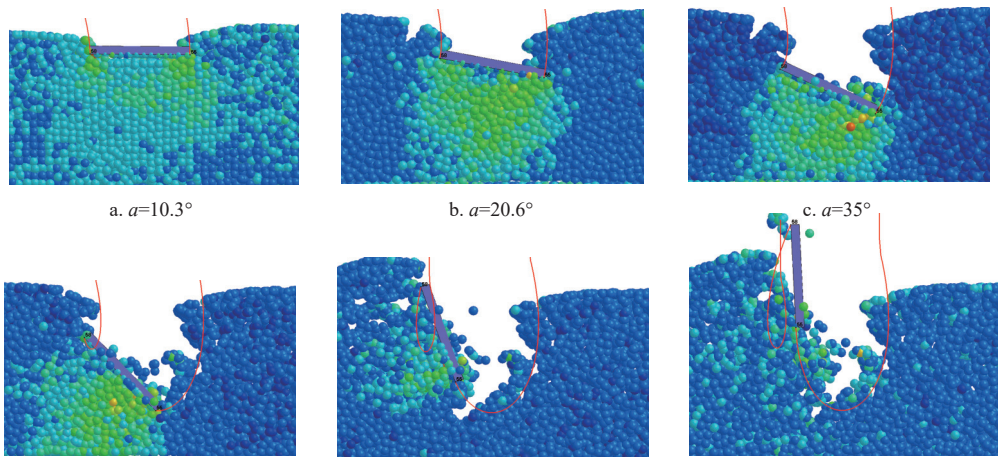

a. a=10.3° b. a=20.6° c. a=35°

d. a=55.69° e. a=80.44° f. a=97°

Figure 11 Screenshot of motion simulation of wheel blade in soil when slip ratio is 26%

above the front and rear ends of the wheel blade partially collapses under the influence of gravity. Then, when the slip rate is 3.1%, with the increase of α, the back end moves forward and upwards, and the front end moves backwards and upwards first, then moves forward and upwards, interacting with the soil. During this period, the soil behind the wheel blade rebounds, the soil stress gradually decreases, and at last the wheel blade pushes the soil forward and upward. When the slip rate is 26%, with the increase of α, the back end of the wheel blade first moves backward and upward, then moves forward and upward, and the front end first moves backward and upward, then moves upward, interacting with the soil. During this period, the soil behind the wheel blade is firstly squeezed and raised by the wheel blade, then the soil rebounds, and the soil stress gradually decreases. When the slip rate is 26%, the wheel blade's crushing and stirring effect on the soil is greater than that of the slip rate of 3.1%. This shows that the slip rate of the tillage wheel is different, the trajectory of the wheel blade and the interaction process between the wheel blade and the soil are different when the slip rate is large, and the wheel blade has a large crushing and stirring effect on the soil.

3.3 Force of single-wheel blade

Figure 12 illustrates the force variations on the single-wheel blade. Figure 12a shows the horizontal thrust, while Figure 12b depicts the support force. The solid line represents the forces at a slip rate of 26%, and the dashed line corresponds to the forces at a slip rate of 3.1%.

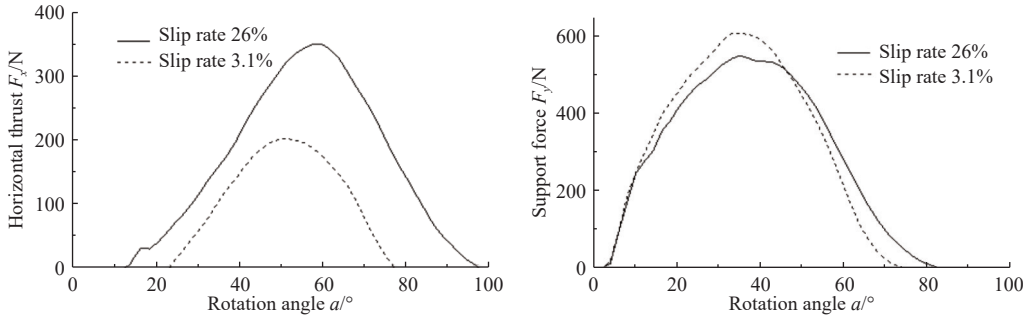

a. Horizontal thrust b. Support force

Figure 12 Force change of a single-wheel blade

As can be seen from Figure 12a, when the slip rate is 3.1% and α is in the range of 0-22.7°, 78.4°-97.0°, and when the slip rate is 26% and α is in the range of 0-14.4°, the horizontal thrusts are negative. The reason is that when α is in these ranges, the horizontal speed of the wheel blade is forward, and the wheel blade pushes the soil forward, so the horizontal thrusts are negative. When the slip rate is 3.1% and α is in the interval of 22.7°-78.4°, and when the slip rate is 26% and α is in the interval of 14.4°-97.0°, with the increase of α, the horizontal thrusts first increase and then decrease. This is the same as the results of previous similar studies[1,9].

It can be seen from Figure 12b that as the α increases, the support forces are first positive value, first increase and then decrease, then negative value, increase first and then decrease. When the slip rate is 3.1% and α is 73.7°, and when the slip rate is 26% and α is 81.5°, the support forces are 0. This shows that the slip rate is different, and the α with the support force of 0 is different, which is the same as in the case of the previous literature[1]. At the same time, as can be seen from Figure 12, when the slip rate is 3.1%, the maximum horizontal thrust and support force of the wheel blade are respectively 202 N and 603 N, and when the slip rate is 26%, the maximum horizontal thrust and support force of the wheel blade are respectively 350 N and 547 N. This shows that the maximum horizontal thrust at the slip rate of 3.1% is 42.28% smaller than the maximum horizontal thrust at the slip rate of 26%. However, the maximum support force at the slip rate of 3.1% is 10% greater than the maximum support force at the slip rate of 26%.

3.4 Regression analysis

The SPSS software was used to perform regression analysis on the test data of Table 3, and the mathematical models of the average forward speed y_1 and stirring degree y_2 of the tillage wheel were obtained, as shown in Equations (5) and (6).

$$y_1 = -2603.278 + 3.073d_1 - 25.715a + 74.864\gamma + 101.153\theta - 0.087d_1\theta + 0.153a^2 - 0.268a\gamma + 1.376an - 0.783\gamma\theta - 3.195\gamma n - 2.185\theta n + 3.786n^2 \quad (5)$$

Table 3 Numerical simulation test scheme and results

Test No.	d_1/mm	a/mm	γ/(°)	θ/(°)	n/piece	y_1/mm·s^{-1}	y_2/%
1	505	80	55	22.5	12	297.77	52.79
2	505	80	55	7.5	8	474.84	20.36
3	505	80	35	22.5	8	245.66	44.67
4	505	80	35	7.5	12	350.52	33.15
5	505	60	55	22.5	8	588.66	26.87
6	505	60	55	7.5	12	499.71	18.75
7	505	60	35	22.5	12	315.14	36.84
8	505	60	35	7.5	8	73.25	53.07
9	435	80	55	22.5	8	326.06	44.93
10	435	80	55	7.5	12	272.91	42.12
11	435	80	35	22.5	12	264.38	40.56
12	435	80	35	7.5	8	81.76	58.14
13	435	60	55	22.5	12	227.59	59.41
14	435	60	55	7.5	8	429.82	24.62
15	435	60	35	22.5	8	210.62	35.85
16	435	60	35	7.5	12	58.74	53.56
17	540	70	45	15.0	10	336.65	33.74
18	400	70	45	15.0	10	198.02	40.22
19	470	90	45	15.0	10	290.38	51.29
20	470	50	45	15.0	10	435.83	36.16
21	470	70	65	15.0	10	619.26	24.12
22	470	70	25	15.0	10	1.24	55.56
23	470	70	45	30.0	10	306.60	44.12
24	470	70	45	0.0	10	265.44	29.98
25	470	70	45	15.0	14	302.43	35.39
26	470	70	45	15.0	6	409.60	29.05
27	470	70	45	15.0	10	269.96	43.65
28	470	70	45	15.0	10	269.96	43.65
29	470	70	45	15.0	10	269.96	43.65
30	470	70	45	15.0	10	269.96	43.65
31	470	70	45	15.0	10	269.96	43.65
32	470	70	45	15.0	10	269.96	43.65
33	470	70	45	15.0	10	269.96	43.65
34	470	70	45	15.0	10	269.96	43.65
35	470	70	45	15.0	10	269.96	43.65
36	470	70	45	15.0	10	269.96	43.65

$$y_2 = 201.174 - 5.245\gamma - 12.431\theta + 15.52n + 0.011d_1\theta - 0.029d_1n + 0.010a^2 - 0.112an + 0.112\gamma\theta + 0.295\gamma n + 0.235\theta n - 0.512n^2 \quad (6)$$

The significance test results of the mathematical models and regression coefficients show that the models are significant at the level of 0.0001 and the coefficients are significant at the level of 0.063 to 0.0001. The influence of the test factors are highly significant. The mathematical models developed in this study can be used in research on the influence of the operational quality of the tillage wheel.

3.5 Influence analysis of factors

According to Equations (5) and (6), the relation figure between the factor interactions and y_1, y_2 was obtained by using Matlab software, as shown in Figure13. In addition to the factors

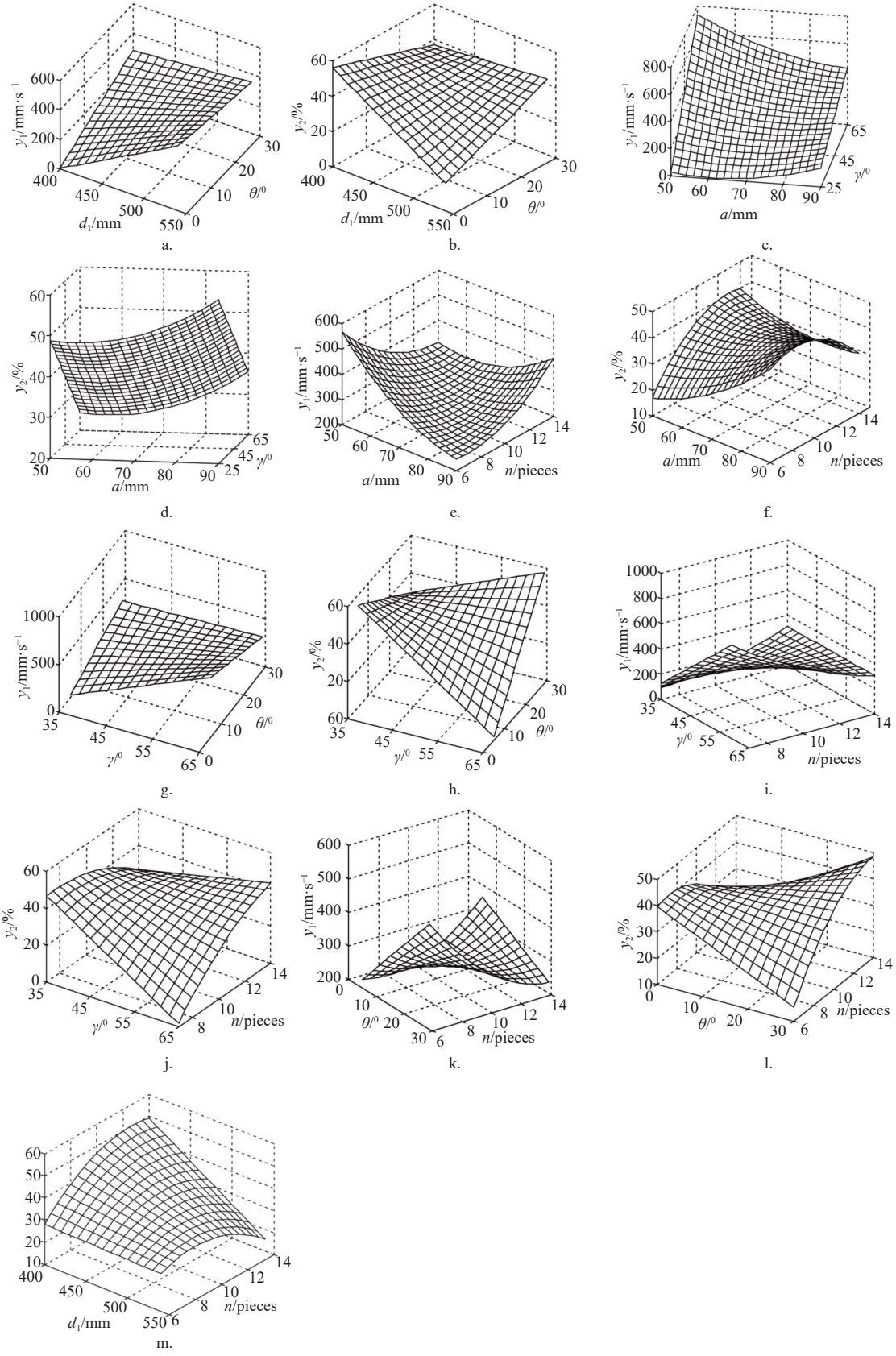

Figure 13 Relation curves between factor interactions and experiment indices

considered in the calculation, other factors were zero level values.

It can be seen from Figure13a and 13b, under the combination that d_1 is 400 mm and θ is 0, y_1 is the smallest, with a value of 4.30 mm/s, and y_2 is the largest, with a value of 56.50%. When d_1 is 550 mm and θ is 0, y_1 is the largest, with a value of 465.25 mm/s, and y_2 is the smallest, with a value of 13%. As d_1 increases, y_1 increases. When θ is less than 27°, y_2 decreases as d_1 increases, and when θ is greater than 27°, y_2 increases slightly as d_1 increases. When d_1 is less than 450 mm, as θ increases, y_1 increases, and y_2 decreases; when d_1 is greater than 450 mm, as θ increases, y_1 decreases and y_2 increases.

It can be seen from Figure 13c and 13d, under the combination that a is 60 mm and γ is 25°, y_1 is the smallest, with a value of 6.55 mm/s. When a is 90 mm and γ is 25°, y_2 is the largest, with a value of 60.03%. When a is 50 mm and γ is 65°, y_1 is the largest, with a value of 735.56 mm/s. When a is 56 mm and γ is 65°, y_2 is the smallest, with a value of 23.87%. As a increases, y_1 and y_2 exhibit a parabola change with a concave upward. As γ increases, y_1 increases and y_2 decreases.

It can be seen from Figure13e and 13f, under the combination that a is 50 mm and n is 6, y_1 is the largest, with a value of 568.88 mm/s, and y_2 is the smallest, with a value of 16.94%. When a is 90 mm and n is 7, y_1 is the smallest, with a value of 241.43 mm/s. When a is 90 mm and n is 9, y_2 is the largest, with a value of 48.85%. As a increases, y_1 and y_2 exhibit a parabola change with a concave upward. As n increases, y_1 exhibits a parabolic variation with an upward-facing concave, and y_2 exhibits a parabolic variation with a downward-facing concave .

It can be seen from Figure13g and 13h, under the combination that γ is 65° and θ is 5°, y_1 is the largest, with a value of 702.49 mm/s, and y_2 is the smallest, with a value of 2.14%. When γ is 35° and θ is 5°, y_1 is the smallest, with a value of 32.91 mm/s. When γ is 65° and θ is 29°, y_2 is the largest, with a value of 59 %. When θ is less than 15°, as γ increases, y_1 increases and y_2 decreases. When θ is greater than 15°, y_1 increases and y_2 also increases. When γ is less than 40°, as θ increases, y_1 increases and y_2 decreases. When γ is greater than 40°, as θ increases, y_1 decreases and y_2 increases.

It can be seen from Figure 13i and 13j, under the combination that γ is 65° and n is 7, y_1 is the largest, with a value of 754.57 mm/s, and y_2 is the smallest, with a value of 1.7%. When γ is 35° and n is 7, y_1 is the smallest, with a value of 94.75 mm/s, and y_2 is the largest, with a value of 46.7%. When n is less than 12, as γ increases, y_1 increases and y_2 decreases. When n is greater than 12, as γ increases, y_1 is basically unchanged, and y_2 is increased. As n increases, y_1 exhibits a parabolic change with a concave face up, and y_2 exhibits a parabolic change with a concave face down.

It can be seen from Figure 13k and 13l, under the combination that θ is 30° and n is 6, y_1 is the largest, with a value of 524.47 mm/s, and y_2 is the smallest, with a value of 15.34%. When θ is 0° and n is 6, y_1 is the smallest, with a value of 166.93 mm/s. When θ is 30° and n is 14, y_2 is the largest, with a value of 48.42%. When n is less than 10, as θ increases, y_1 increases and y_2 decreases. When n is greater than 10, as θ increases, y_1 decreases and y_2 increases. As n increases, y_1 exhibits a parabolic change with a concave face up, and y_2 exhibits a parabolic change with a concave face down.

As can be seen from Figure 13m, under the combination that d_1 is 400 mm and n is 13, y_2 is the largest, with a value of 50.20%. As d_1 increases, y_2 decreases, and as n increases, y_2 exhibits a parabolic change with a concave face down.

4 Conclusions

A simulation model of soil-tillage wheel system using SPH method and field tests was established and verified. The mathematical models of tillage wheel performance influenced by multiple factors were developed through a quadratic regression orthogonal rotation design and regression analysis. The movement of a single-wheel blade in soil, its interaction with the soil, the forces acting on it, and the impacts of various factors on the operational performance of the tillage wheel were studied. The major conclusions are drawn as follows:

a) The field verification test shows that the modeling method of the soil-tillage wheel system based on SPH method is reasonable. The established model can effectively be used for simulating tillage wheel operations.

b) When the slip rate is different, the trajectory of the wheel blade and the interaction process between the wheel blade and the soil are different. When the slip rate is large, the wheel blade has a large effect on the crushing and stirring of the soil. As the rotation angle α increases, the horizontal thrust and support force of the wheel blade first increase and then decrease. When the slip rate is different, the rotation angle α with the support force of 0 is different. When the slip rates are 3.1% and 26%, the α with the support force of 0 are 73.7° and 81.5°, respectively. The maximum horizontal thrust at the slip rate of 3.1% is 42.28% smaller than the maximum horizontal thrust at the slip rate of 26%. The maximum support force at the slip rate of 3.1% is 10% greater than the maximum support force at the slip rate of 26%.

c) As the outer diameter d_1 of the rim or the inclination angle γ increases, the average forward speed y_1 increases, and the stirring degree y_2 decreases. As the width a or the number n of the wheel blades increases, the average forward speed y_1 shows a parabolic change with a concave upward. As the wheel blade width a increases, the stirring degree y_2 shows a parabolic change with a concave upward. As the number n of the wheel blades increases, the stirring degree y_2 shows a parabolic change with a concave face down. When small d_1 or small n or small γ is combined with θ, as θ increases, y_1 increases and y_2 decreases, and vice versa.

d) It is suggested to use the established mathematical models of operational performance, combined with the interaction analysis between the wheel blade and the soil, to optimize the design of the tillage wheel and improve its operational performance.

Acknowledgements

This work was supported by grants from the National Natural Science Foundation of China (Grant No. 32160422), the Guangxi Science and Technology Major Program (Grant No. Guike AA23073003), and the Guangxi Natural Science Foundation (Grant No. 2023GXNSFAA026376).

[References]

[1] Shao Y J, Luo X W. The design and performance test on lug wheel for powered tiller. Transactions of the CSAE, 1992; 8(2): 80–87. (in Chinese)

[2] Shao Y J, Zhou D J, Luo X W. Simulated experiment on the dynamics of lug wheel with the lugs stepping along the previous rut and cavities. Transactions of the CSAE, 1995; 11(1): 58–64. (in Chinese)

[3] Salokhe V M, Manzoor S, Gee-Clough D. Pull and lift forces acting on single cage wheel lugs. Journal of Terramechanics, 1990; 27(1): 25–39.

[4] Lu H Z, Shao Y J, Luo X W. Experiment and research on the dynamic performance of a single lug. Transactions of the CSAE, 1995; 11(1): 65–70. (in Chinese)

[5] Hermawan W, Yamazaki M, Oida A. Theoretical analysis of soil reaction on a lug of the movable lug cage wheel. Journal of Terramechanics, 2000;

37(2): 65–86.
[6] Watyotha C, Gee-Clough D, Salokhe V M. Effect of circumferential angle, lug spacing and slip on lug wheel forces. Journal of Terramechanices, 2001; 38(1): 1–14.
[7] Hendriadi A, Salokhe V M. Improvement of a power tiller cage wheel for use in swampy peat soils. Journal of Terramechanics, 2002; 39(2): 55–70.
[8] Fajardo A L, Suministrado D C, Peralta E K, Bato P M, Paningbatan Jr E P. Force and puddling characteristics of the tilling wheel of float-assisted tillers at different lug angle and shaft speed. Soil and Tillage Research, 2014; 140(5): 118–125.
[9] Lu H Z, Luo X W. Soil flow rule and dynamic performance under a paddy-field wheel lug. Transactions of the CSAM, 2010; 41(7): 50–53. (in Chinese)
[10] Zhu Z. A new type of micro-tiller. 2014; CN201310003607.0.
[11] Naderi-Boldaji M, Karparvarfard S H, Azimi-Nejadian H. Investigation of the predictability of mouldboard plough draught from soil mechanical strength (cone index *vs*. shear strength) using finite element modelling. Journal of Terramechanics, 2023; 108: 21–31.
[12] Zhang S L, Zhao W Y, Dai F, Song X F, Qu J F, Zhang F W. Simulation analysis and test on suppression operation process of ridging and film covering machine with full-film double-furrow. Transactions of the CSAE, 2020; 36(1): 20–30. (in Chinese)
[13] Kim Y-S, Siddique Md A A, Kim W-S, Kim Y-J, Lee S-D, Lee D-K, et al. DEM simulation for draft force prediction of moldboard plow according to the tillage depth in cohesive soil. Computers and Electronics in Agriculture, 2021; 189: 106368.
[14] Hoseinian S H, Hemmat A, Esehaghbeygi A, Shahgoli G, Baghbanan A. Development of a dual sideway-share subsurface tillage implement: Part 1: Modeling tool interaction with soil using DEM. Soil and Tillage Research, 2022; 215: 105201.
[15] Chen G B, Wang Q J, Li H W, He J, Wang X H, Zhang X Y, He D. Experimental research on vertical straw cleaning and soil tillage device based on Soil-Straw composite model. Computers and Electronics in Agriculture, 2024; 216: 108510.
[16] Kešner A, Chotěborský R, Linda M, Hromasová M, Katinas E, Sutanto H. Stress distribution on a soil tillage machine frame segment with a chisel shank simulated using discrete element and finite element methods and validate by experiment. Biosystems Engineering, 2021; 209: 125–138.
[17] Azimi-Nejadian H, Karparvarfard S H, Naderi-Boldaji M. Weed seed burial as affected by mouldboard design parameters, ploughing depth and speed: DEM simulations and experimental validation. Biosystems Engineering, 2022; 216: 79–92.
[18] Jin X M, Ma F P, Wang D, Zhu Z T. Simulation of mouldboard plough soil cutting based on Smooth Particle Hydrodynamics Method and FEM–SPH coupling method. Agriculture, 2023; 13(9): 1847.
[19] Zhang X Y, Hu X, Zhang L X, Kheiry A N O. Simulation and structural parameter optimization of rotary blade cutting soil based on SPH method. Int J Agric & Biol Eng, 2024; 17(3): 82–90.
[20] Hu M, Gao T, Dong X W, Tan Q T, Yi C, Wu F, et al. Simulation of soil-tool interaction using smoothed particle hydrodynamics (SPH). Soil and Tillage Research, 2023; 229: 105671.
[21] Yang W, Yang ., Jia F Y, Wang Y Q, Huang Y Q. Numerical simulation of digging operation of cassava root planted in red clay. Journal of Mechanical Engineering, 2013; 49(9): 135–143. (in Chinese)
[22] Han Y J, Li Y W, Zhao H H, Chen H, Liu D X. Simulation of soil cutting by vertical rotary blade based on SPH method. Journal of Southwest University (Natural Science Edition), 2016; 38(12): 150–155. (in Chinese)
[23] Kang J M, Li S J, Yang X J, Liu L J, Li C R. Experimental verification and simulation analysis on power consumption of disc type ditcher. Transactions of the CSAE, 2016; 32(13): 8–15. (in Chinese)
[24] Yang W, Zhao W J, Liu Y D, Chen Y Q, Yang J. Simulation of forces acting on the cutter blade surfaces and root system of sugarcane using FEM and SPH coupled method. Computers and Electronics in Agriculture, 2021; 180: 105893.
[25] Tagar A A, Ji C Y, Adamowski J, Malard J, Chen S Q, Ding Q S, et al. Finite element simulation of soil failure patterns under soil bin and field testing conditions. Soil Tillage Research, 2015; 145: 157–170.
[26] Yang W, Xiao X, Pan R H, Guo S Y, Yang J. Numerical simulation of spiral cutter-soil interaction in deep vertical rotary tillage. Agriculture, 2023; 13(9): 1850.
[27] Dun G Q, Chen H T, Li A, Feng Y N, Yang J L, Ji W Y. Effect of rotation direction of knife teeth configuration on clearing straw unit performance for no-tillage and straw mulching precision seeder. Transactions of the CSAE, 2015; 31(12): 48–56. (in Chinese)
[28] Qi L, Liang Z W, Ma X, Tang Y X, Jiang L K. Validation and analysis of fluid-structure interaction between rotary harrow weeding roll and paddy soil. Transactions of the CSAE, 2015; 31(5): 29–37. (in Chinese)
[29] Xie L, Cai M. Finite element analysis and simulation of ANSYS. (2nd ed.). Beijing: Publishing House of Electronics Industry. 2013. 418p.